

The impact of helical flow on coronary atherosclerotic plaque development

*Original*

The impact of helical flow on coronary atherosclerotic plaque development / De Nisco, G.; Hoogendoorn, A.; Chiastra, C.; Gallo, D.; Kok, A. M.; Morbiducci, U.; Wentzel, J. J.. - In: ATHEROSCLEROSIS. - ISSN 0021-9150. - STAMPA. - 300:(2020), pp. 39-46. [10.1016/j.atherosclerosis.2020.01.027]

*Availability:*

This version is available at: 11583/2819154 since: 2020-05-04T16:00:49Z

*Publisher:*

Elsevier Ireland Ltd

*Published*

DOI:10.1016/j.atherosclerosis.2020.01.027

*Terms of use:*

This article is made available under terms and conditions as specified in the corresponding bibliographic description in the repository

*Publisher copyright*

Elsevier postprint/Author's Accepted Manuscript

© 2020. This manuscript version is made available under the CC-BY-NC-ND 4.0 license  
<http://creativecommons.org/licenses/by-nc-nd/4.0/>. The final authenticated version is available online at:  
<http://dx.doi.org/10.1016/j.atherosclerosis.2020.01.027>

(Article begins on next page)

# The Impact of Helical Flow on Coronary Atherosclerotic Plaque Development

Giuseppe De Nisco<sup>a</sup>, Ayla Hoogendoorn<sup>b</sup>, Claudio Chiastra<sup>a</sup>,

Diego Gallo<sup>a</sup>, Annette M. Kok<sup>b</sup>, Umberto Morbiducci<sup>a</sup>, Jolanda J. Wentzel<sup>b</sup>

<sup>a</sup> *PoliTo<sup>BIO</sup>Med Lab, Department of Mechanical and Aerospace Engineering, Politecnico di Torino, 10129 Turin, Italy*

<sup>b</sup> *Department of Cardiology, Biomedical Engineering, Erasmus MC, 3000 CA Rotterdam, The Netherlands*

*The final publication is available online*

**DOI:** <https://doi.org/10.1016/j.atherosclerosis.2020.01.027>

## Corresponding author:

Jolanda J. Wentzel, Dr. Molewaterplein 40, 3015 GD Rotterdam, The Netherlands

P.O. Box 2040, 3000 CA Rotterdam, The Netherlands

Phone: +31107044044; Fax: +31107044720; [j.wentzel@erasmusmc.nl](mailto:j.wentzel@erasmusmc.nl)

**Number of figures:** 5

28    **Abstract**

29    **Background and aims** - Atherosclerosis has been associated with near wall hemodynamics and  
30    wall shear stress (WSS). However, the role of coronary intravascular hemodynamics, in particular  
31    of the helical flow (HF) patterns that physiologically develop in those arteries, is rarely considered.  
32    The purpose of this study was to assess how HF affects coronary plaque initiation and progression,  
33    definitively demonstrating its atheroprotective nature.

34    **Methods** - The three main coronary arteries of five adult mini-pigs on a high fat diet were imaged  
35    by computed coronary tomography angiography (CCTA) and intravascular ultrasound (IVUS) at 3  
36    (T1, baseline) and 9.4±1.9 (T2) months follow-up. The baseline geometries of imaged coronary  
37    arteries (n=15) were reconstructed, and pig-specific computational fluid dynamic simulations were  
38    performed. Local wall thickness (WT) was measured on IVUS images at T1 and T2, and its temporal  
39    changes were assessed. Descriptors of HF and WSS nature were computed for each model, and  
40    statistically compared to WT data.

41    **Results** - HF intensity was strongly positively associated with WSS magnitude ( $p<0.001$ ). Overall,  
42    coronary segments exposed to high baseline levels of HF intensity exhibited a significantly lower  
43    WT growth ( $p<0.05$ ), compared to regions with either mid or low HF intensity.

44    **Conclusions** - This study confirms the physiological significance of HF in coronary arteries,  
45    revealing its protective role against atherosclerotic WT growth and its potential in predicting  
46    regions undergoing WT development. These findings support future *in vivo* measurement of  
47    coronary HF as surrogate atherosclerotic risk marker, overcoming current limitations of *in vivo*  
48    WSS assessment.

49    **Keywords:** Atherosclerosis; Computational fluid dynamics; Wall shear stress; plaque progression.

50     **Introduction**

51     Coronary atherosclerosis is a complex and multifactorial disease, influenced by local biological,  
52     biomechanical, and systemic factors [1,2]. The underlying mechanisms of the transformation from  
53     a healthy to a diseased coronary artery are still incompletely understood. As a consequence, a  
54     robust arsenal of predictive tools for this mostly asymptomatic disease has not been identified yet.  
55     Among the biomechanical factors that promote atherosclerotic plaque onset and progression in  
56     coronary arteries, local hemodynamics plays a major role [2,3]. In particular, low wall shear stress  
57     (WSS) is widely recognized as an independent, albeit moderate, predictor of plaque development  
58     [4,5].

59             Besides the widely investigated WSS, physiological helical flow (HF) has also been  
60     hypothesized to have a relevant impact on vascular disease. HF, consisting of a helical-shaped  
61     arrangement of the streaming blood (as given by the combination of translational and rotational  
62     blood flow motions), is known to markedly characterize arterial hemodynamics [6-9]. The  
63     physiological significance of arterial HF, in particular its atheroprotective nature, has emerged in  
64     the last decade in the human aorta [6,10-12] and in the human carotid bifurcation [13-15]. All  
65     those studies highlighted the role played by HF in mitigating near-wall flow disturbances, thereby  
66     suppressing the area exposed to low WSS, which protects from atherosclerosis development [2].

67             Very recently, we showed the existence of distinguishable HF flow features in coronary  
68     arteries. These HF features were hypothesized to be atheroprotective, as our data demonstrated a  
69     strong association between HF and the luminal surface area exposed to low, proatherogenic WSS  
70     [16].

71     Following these recent findings, the final goal of this study was to demonstrate the protective role  
72     of HF for atherosclerotic plaque development over time. Findings from this work would contribute  
73     (1) to further clarify the physiological significance of HF in coronary arteries, and (2) to the debate

74 on a possible future use of HF-based hemodynamic descriptors as *in vivo* surrogate markers of  
75 WSS for diagnostic/prognostic purposes overcoming current limitations and inaccuracies related  
76 to the direct measurement of WSS from *in vivo* imaging [\[17\]](#).

## 77 **Materials and Methods**

### 78 *Animal population and imaging*

79 Five adult familial hypercholesterolemia Bretoncelles Meishan mini-pigs with a mutation in the  
80 low-density lipoprotein receptor (*LDLR*) (age of  $34\pm 3$  months, castrated male) were put on a high  
81 fat diet to trigger atherosclerosis development. As described in detail elsewhere [16,18], the  
82 animals underwent computed coronary tomography angiography (CCTA) and intravascular  
83 ultrasound (IVUS) imaging of the three main coronary arteries (left anterior descending - LAD, left  
84 circumflex - LCX, and right coronary artery - RCA). The imaging protocol was performed at 3  
85 months after the start of the diet (T1, considered as the baseline in this study), and after  $9.4\pm 1.9$   
86 months (T2). At T1, Doppler-based blood flow velocity measurements were recorded in each  
87 artery at the inflow section and immediately upstream and downstream of each side branch, using  
88 the ComboWire (Volcano Corp., Rancho Cordova, CA, USA). An overview of the methods is  
89 provided in Figure 1. In addition, some classical risk factors were measured in the 5 investigated  
90 animals including weight, leukocytes, Total cholesterol, LDL-C, HDL-C and LDL-C/HDL-C ratio.  
91 The study was performed according to the National Institute of Health guide for the Care and Use  
92 of Laboratory animals [19]. Ethical approval was obtained from the local animal ethics committee  
93 of the Erasmus MC (EMC nr. 109-14-10).

### 94 *Plaque growth measurements*

95 To quantify the local wall thickness (WT), the lumen and vessel wall contour of each of the 15  
96 investigated coronary arteries (5 LAD, 5 LCX and 5 RCA, Figure S1 of the Supplementary Materials)  
97 were semi-automatically detected on IVUS images at T1 and at T2 using QCU-CMS software  
98 (version 4.69, Leiden University Medical Centre, LKEB, Division of Image Processing), as depicted in  
99 Figure 2. WT was assessed by subtracting the distance between the lumen center and the outer

100 wall contour, from the distance to the lumen contour. Plaque development over time was  
101 quantified in terms of change in WT ( $\Delta$ WT) between time points T1 and T2. The  $\Delta$ WT was then  
102 adjusted for the number of months between both time points for the individual pigs, resulting in a  
103 measure of  $\Delta$ WT/month. WT measurements were averaged over 3mm/45 degrees sectors of the  
104 luminal surface (Figure 2) in order to capture the local effects of HF on plaque development.

#### 105 *Computational hemodynamics*

106 The 3D geometry of coronary arteries at T1 was reconstructed by stacking segmented IVUS lumen  
107 contours on the CCTA 3D centerline using Mevislab (Bremen, Germany), as described in detail  
108 elsewhere [16]. Unsteady-state CFD simulations were performed on the reconstructed geometries  
109 to quantify near-wall and intravascular hemodynamic features. The finite volume method was  
110 used to numerically solve the governing equations of fluid motion. Blood was assumed as an  
111 incompressible, homogeneous, non-Newtonian fluid. No-slip condition was assumed at the  
112 arterial wall. Personalized boundary conditions were derived from individual *in vivo* velocity  
113 ComboWire Doppler measurements at several locations along the vessel. The most proximal  
114 measurement was used to estimate the flow rate value, prescribed as inlet boundary condition in  
115 terms of time-dependent flat velocity profile. At each side branch, the measured flow ratio was  
116 estimated as the difference between upstream and downstream velocity-based flow rate  
117 measurements and applied as outflow condition. If flow velocity measurements were inaccurate  
118 or not available, a diameter-based scaling law [20] was applied to estimate the flow ratio [16].

#### 119 *Hemodynamic descriptors*

120 The hemodynamic descriptors considered for the analysis are listed in Figure 2 (see Table S2 of the  
121 Supplementary Materials for their mathematical formulation). In short, helical flow in the 15  
122 coronary artery models at T1 was assessed in terms of average helicity intensity ( $h_2$ ), which gives a  
123 measure of the strength of the pitch and torsion of coronary blood flow and is given by the cardiac

124 cycle- and volume-averaged value of the unsigned internal product of local velocity and vorticity  
125 vectors [13]. In this work, to characterize each coronary model with a representative helicity  
126 intensity value,  $h_2$  was analyzed in the near-wall volume (i.e., defined by the outer 10% of the local  
127 radius) and in the whole volume (i.e., defined by the entire local radius) of the main vessel.  
128 Moreover, helicity intensity data were calculated over 3mm/45 degrees sectors, considering both  
129 near-wall and entire local radius volumes. The consideration of the near-wall volume was  
130 motivated by the recently observed link between HF and WSS patterns perpendicular to the  
131 centerline of coronary arteries, quantified by the so-called secondary WSS [16]. In addition, the  
132 local normalized helicity (LNH) [21] was adopted to visualize right- and left-handed helical fluid  
133 patterns inside coronary arteries (respectively, positive and negative LNH values, [11].

134 To complement the HF characterization, the luminal distribution of time-averaged wall shear  
135 stress (TAWSS) and of three descriptors of WSS multidirectionality were evaluated at baseline  
136 (Figure 2, Table S2). In short, WSS multidirectionality was described considering two projections of  
137 WSS vector [22]: (1) along the centerline of the artery, defining the “axial direction” ( $\mathbf{WSS}_{ax}$ ); (2)  
138 perpendicular to the centerline, defining the secondary direction ( $\mathbf{WSS}_{sc}$ ). The  $\mathbf{WSS}_{ax}$  and  $\mathbf{WSS}_{sc}$   
139 local vectors were averaged over the cardiac cycle (Avg $\mathbf{WSS}_{ax}$  and Avg $\mathbf{WSS}_{sc}$ , respectively).  
140 Moreover, their cycle-average magnitude was evaluated (TAWSS $_{ax}$  and TAWSS $_{sc}$ , respectively). To  
141 detect regions at the luminal surface where the local secondary WSS component predominates  
142 over the axial one, the ratio of the secondary to axial  $\mathbf{WSS}$  magnitudes (WSS $_{ratio}$ ) was computed  
143 [22]. The WSS-based descriptors were also averaged over the same 3mm/45 degrees sectors at  
144 the luminal surface as WT data.

#### 145 *Statistical analysis*

146 The existence of possible associations between WSS and HF was investigated considering the  
147 average values of the WSS-based descriptors and the helicity-based descriptor  $h_2$  over each



148 individual coronary artery. Regression analysis was used to identify relations between each pair of  
149 hemodynamic descriptors and reported as Spearman correlation coefficients.

150 The analysis of the relation between plaque growth and hemodynamic descriptors was conducted  
151 using the sector-based data applying a mixed model with hemodynamic descriptors as fixed  
152 factors, the individual vessel as random factor to correct for clustering of the analyzed sectors per  
153 vessel and the average cholesterol levels as covariate (IBM SPSS Statistics, version 24.0). The  
154 values of the hemodynamic descriptors were classified as low, mid or high, based on artery-  
155 specific tertile-division. Statistical significance was assumed for  $p<0.05$ .

## 156 Results

157 Classical cardiovascular risk factors, weight, leukocytes, cholesterol, LDL-C, HDL-C and LDL-C/HDL-C  
158 ratio did not significantly change over time for the investigated 5 pigs and are presented in Table  
159 S1 of the Supplementary Materials.

### 160 *Coronary hemodynamics: general observations*

161 For each investigated coronary artery model, the distribution of the WSS-based descriptors was  
162 assessed, as shown for a representative case in Figure 3 (panels A-D). A similar approach was used  
163 for studying the HF features: the LNH red and blue colors indicate right-handed and left-handed  
164 HF patterns, respectively. Thereby, the presence of two distinguishable counter-rotating HF  
165 patterns was observed in this case (Figure 3-E) and reflects the arrangement in counter-rotating  
166 helical structures in all coronary arteries.

167 Figure 3-A shows the luminal distribution of TAWSS highlighting, as expected, the presence of  
168 case-specific focal low TAWSS regions located at the distal portion of the main branch.  
169 Furthermore, the figure shows in the other panels (B-D) that WSS was predominantly aligned with  
170 the forward flow direction (i.e., positive Avg**WSS**<sub>ax</sub> values), which was representative for all cases.  
171 Moreover, it emerged that the organization of coronary blood flow in two counter-rotating helical  
172 structures, which is evident from LNH visualization, influences the near-wall hemodynamics of  
173 coronary vessels. Considering the coronary artery depicted in Figure 3-D, positive/negative values  
174 of Avg**WSS**<sub>sc</sub>, indicating left-handed and right-handed directions respectively, resemble the  
175 rotating direction of helical flow structures given by the LNH (Figure 3-E). In addition, the analysis  
176 of the luminal distributions of the **WSS**<sub>ratio</sub> revealed that **WSS** in the axial direction (**WSS**<sub>ax</sub>) was  
177 dominant over the **WSS** perpendicular to the vessel centerline (**WSS**<sub>sc</sub>). In fact, the **WSS**<sub>ratio</sub> was <1

178 over most of the lumen of all the investigated coronary arteries (around 94% of the investigated  
179 luminal surface sectors, see also Figure 3-B).

#### 180 *Link between hemodynamic variables*

181 Regression analysis revealed a significant association between the average values of the WSS-  
182 based descriptors and helicity intensity  $h_2$  of each individual coronary artery (Figure 3-F). In detail,  
183 TAWSS was strongly and positively associated with both whole volume  $h_2$  ( $r=0.925$ ,  $p<0.001$ ) and  
184 near-wall  $h_2$  ( $r=0.629$ ,  $p<0.01$ ), indicating that the higher the helicity intensity ( $h_2$ ) is, the higher is  
185 the TAWSS value. Moreover, positive, significant associations emerged between the whole volume  
186  $h_2$ , and both  $TAWSS_{ax}$  ( $r=0.843$ ,  $p<0.001$ ) and  $TAWSS_{sc}$  ( $r=0.843$ ,  $p<0.001$ ). A weaker, but still  
187 significant, direct association emerged between near-wall  $h_2$  and  $TAWSS_{ax}$  ( $r=0.629$ ,  $p<0.05$ ). Only  
188 a near-significant association was observed for the near-wall  $h_2$  and  $TAWSS_{sc}$  ( $r=0.468$ ,  $p=0.081$ ).  
189 These results suggest a predominant role for HF intensity in the whole intraluminal volume, rather  
190 than only near-wall, in determining secondary **WSS** magnitude. Last, a direct, significant  
191 association between the whole volume  $h_2$  and  $WSS_{ratio}$  ( $r=0.757$ ,  $p<0.01$ ) emerged, but no  
192 significant association was observed for the latter with near-wall  $h_2$ .

#### 193 *Link between hemodynamic variables and increase in wall thickness*

194 Overall, the 15 pig coronary arteries presented a marked increase in average WT over the follow-  
195 up period (WT at T1 =  $0.183 \pm 0.108$  mm, WT at T2 =  $0.427 \pm 0.313$  mm;  $p<0.001$ ).

196 Coronary sectors exposed to low TAWSS exhibited a significantly larger  $\Delta WT$  per month ( $0.048 \pm$   
197  $0.007$  mm/month) compared to regions with either mid ( $\Delta WT/month = 0.035 \pm 0.007$  mm/month)  
198 or high ( $\Delta WT/month = 0.027 \pm 0.007$  mm/month) TAWSS values (Figure 4 - top panel). The analysis  
199 revealed a significant, inverse association between HF and WT progression. In particular (Figure 4 -  
200 top panel), in luminal sectors where near-wall  $h_2$  was high, significantly low WT growth rate ( $0.032$   
201  $\pm 0.007$  mm/month) was observed, compared to luminal sectors with either mid ( $\Delta WT/month =$

202 0.037  $\pm$  0.007 mm/month) or low ( $\Delta$ WT/month = 0.040  $\pm$  0.007 mm/month) near-wall  $h_2$ . A similar  
203 relation emerged for  $h_2$ . Among the investigated descriptors of WSS directionality, only high  
204 TAWSS<sub>ax</sub> was significantly associated with lower WT progression (0.030  $\pm$  0.002 mm/month for the  
205 highest TAWSS<sub>ax</sub> tertile).

206 In addition, the results of the time-specific statistical analysis are reported in Figure 4 (T1 - mid  
207 panel; T2 - bottom panel). In detail, the association between  $h_2$  and WT at T1 was only near  
208 significant ( $p=0.06$ ), while no significant association emerged between near-wall  $h_2$  and measured  
209 WT at T1 (Figure 4 - mid panel). As for WSS distribution, luminal sectors exposed to high TAWSS at  
210 T1 significantly displayed the lowest T1 WT values. Similar results (but with smaller standard  
211 errors), were observed for TAWSS<sub>ax</sub>. However, neither TAWSS<sub>sc</sub> nor WSS<sub>ratio</sub> were significantly  
212 associated with WT at T1. The analysis of the relations between hemodynamic descriptors at T1  
213 and WT at T2 revealed similar results to those found for the overall WT growth per month  
214 between T1 and T2 (Figure 4 - lower panel). In contrast to the  $\Delta$ WT/month analysis, in the analysis  
215 of WT at T2, luminal sectors exposed to higher TAWSS<sub>sc</sub> values at T1 exhibited significantly lower  
216 WT values at T2.

## 217 Discussion

### 218 *Summary of findings and their implications*

219 In the present study, we investigated the association between local hemodynamics and  
220 atherosclerosis progression in a representative dataset of 15 pig coronary arteries. The study  
221 highlighted the existence of a clear association between HF intensity ( $h_2$ ) at baseline and plaque  
222 development over time in coronary arteries. In detail, sectors at the luminal surface with the  
223 lowest WT growth rate values were preceded by higher baseline values of helicity intensity,  
224 suggesting a beneficial role of the HF patterns in coronary arteries. The atheroprotective role of HF  
225 was confirmed when extending the analysis to WSS, a factor known to be involved in  
226 atherosclerotic disease [23]. These findings confirm and strengthen our previously reported  
227 associations between helicity intensity and WSS-based hemodynamic descriptors in coronary  
228 arteries [16].

229 A schematic of the main findings is reported in Figure 5 to summarize the hemodynamics-related  
230 mechanisms that might be involved in atherosclerotic disease progression: (1) helical blood flow  
231 patterns characterized by high helicity intensity ( $h_2$ ) stabilize coronary hemodynamics, thus reduce  
232 flow disturbances resulting in more atheroprotective WSS levels at the luminal surface (e.g., Figure  
233 3-F); (2) atheroprotective WSS values maintain endothelial cells (EC) quiescence and junctions  
234 stability [3,23,24], contributing to prevent plaque initiation. The already highlighted role of low  
235 WSS as predictor of plaque development in coronary vessels [3,5,24] also clearly emerged in this  
236 study (Figure 4 - top panel). In detail, low baseline values of TAWSS, which are associated to a low  
237 HF intensity (Figure 3-F), might trigger biological mechanisms, i.e., EC polygonal shaping, pro-  
238 atherogenic genes upregulation, nitric oxide reduction inducing EC dysfunction [3,23,24],  
239 promoting the atherogenic plaque onset and faster disease development.

240 In this study the commonly used multidirectional WSS metric oscillatory shear index (OSI) was not  
241 analyzed since previous studies demonstrated that coronary arteries develop very low OSI values  
242 [16,18]. Moreover, the already observed scarce multidirectionality of WSS in coronary vessels [16]  
243 was confirmed here by assessing its axial and secondary components. The  $WSS_{ratio}$  assumed values  
244 lower than 1 over most of the lumen of all the investigated coronary arteries, indicating that the  
245 WSS is markedly aligned with the main flow direction (see explanatory case in Figure 3-B).  
246 The association of hemodynamic quantities with WT at T1 was significant only for TAWSS and  
247  $TAWSS_{ax}$ . Eventhough plaque growth was just initiated; the plaque location showed to comply  
248 with the local TAWSS. Luminal regions exposed to higher  $TAWSS_{sc}$  values were significantly  
249 associated to lower WT at T2, reflecting that high (atheroprotective) values of TAWSS generally  
250 result in higher values of  $TAWSS_{sc}$ .  
251 Furthermore, the findings of this study serve to quantitatively explain for the first time the  
252 irregular helical-shaped distribution of fatty and fibrous plaques in coronary artery reported by  
253 previous ex vivo studies [25-28], and hinted at by the WT patterns shown for the representative  
254 case in Figure 2, where the high WT region seems to follow a helical distribution.

#### 255 *Limitations of the study*

256 Several limitations could weaken the findings of this study. Computational hemodynamic  
257 modelling suffers from assumptions and uncertainties, such us rigid walls and absence of the  
258 cardiac-induced motion of coronary arteries. However, their impact on the WSS distribution has  
259 been demonstrated to be minor, especially when considering time-averaged WSS quantities [29].  
260 Moreover, the findings of the study are based upon a relatively modest number of coronary artery  
261 models (N=15). Nevertheless, the consideration of multiple sectors within each coronary artery  
262 allowed for statistically significant relationships to emerge, capturing the links between local  
263 hemodynamics, WT, and WT progression, when using a linear mixed-effects model correcting for

264 intra-vessel and cholesterol WT dependence. The here adopted division of the hemodynamic  
265 variables in tertiles could be considered arbitrary. However, the lack of established threshold  
266 values justifies this objective and conservative choice. Lastly, this study was carried out on a pig  
267 model. However, the established similarity between pig and human coronary anatomy and  
268 hemodynamics [30] supports the translation of the findings of this study to human coronary  
269 arteries.

270 *Future perspectives*

271 In addition to the causative role of helical flow in determining WSS, a beneficial relation between  
272 HF intensity at baseline and WT and its progression in the follow-up emerged here. Taken  
273 together, these findings suggest that HF intensity may serve as a convenient and pragmatic  
274 surrogate marker of low WSS for prediction of WT progression. Although WSS remains the more  
275 sensitive hemodynamic indicator for atherosclerotic disease, *in vivo* WSS measurements are less  
276 accurate than measurements of intravascular fluid quantities like HF [31]. Furthermore, future  
277 advances in phase-contrast magnetic resonance imaging might extend the feasibility of *in vivo*  
278 arterial helical flow quantitative analysis, already demonstrated for large arteries [6,11,32-34], to  
279 small vessels like the coronary arteries [17,35-39]. This would allow *in vivo*-based prediction of  
280 atherosclerotic disease progression based upon helicity-based descriptors and thereby open a  
281 clinical translation of the relationships reported in this study.

282 *Conclusions*

283 This study in coronary arteries confirms a clear association between helical flow, anti-atherogenic  
284 wall shear stress patterns and protection from plaque progression over time in an atherosclerotic  
285 pig model. In detail, the study confirmed the role of helical blood flow features (in terms of HF  
286 intensity) in conditioning WSS luminal distribution, which in turn interacts with the  
287 pathophysiology of atherosclerotic plaque formation. Due to its role in determining WSS, HF

288 intensity could act as a practical surrogate marker of low WSS and, thus, as a potential  
289 biomechanical predictor of atherosclerotic plaque onset and progression.



290    **Conflict of Interest**

291    The authors state no conflict of interest for the study object of the manuscript. The research was  
292    not supported financially by private companies. None of the authors has a financial agreement  
293    with peoples or organizations that could inappropriately influence their work.

294    **Financial support**

295    Funding was received from the European Research Council under the European Union's Seventh  
296    Framework Programme / ERC Grant Agreement n. 310457.

297    **Author contributions**

298    G.D.N., A.H., C.C, D.G., U.M. and J.J.W.: conception and design of the study; A.H.: acquisition and  
299    analysis of in vivo data; G.D.N. and A.M.K.: computational simulation and analysis of simulation  
300    data; G.D.N, D.G., C.C., U.M., and J.J.W.: drafting of the manuscript. All authors revised the  
301    manuscript critically for important intellectual content and provided final approval for publication.

302     **References**

303     1. Kwak BR, Bäck M, Bochaton-Piallat ML, Caligiuri G, Daemen MJ, Davies PF, Hoefer IE, Holvoet P,  
304         Jo H, Krams R, Lehoux S, Monaco C, Steffens S, Virmani R, Weber C, Wentzel JJ, Evans PC.  
305         Biomechanical factors in atherosclerosis: mechanisms and clinical implications. *Eur Heart J*  
306         2014;35(43):3013-20.

307     2. Morbiducci U, Kok AM, Kwak BR, Stone PH, Steinman DA, Wentzel JJ. Atherosclerosis at arterial  
308         bifurcations: evidence for the role of haemodynamics and geometry. *Thromb Haemost*  
309         2016;115(3):484-92.

310     3. Wentzel JJ, Chatzizisis YS, Gijzen FJH, Giannoglou GD, Feldman CL, Stone PH. Endothelial shear  
311         stress in the evolution of coronary atherosclerotic plaque and vascular remodelling: current  
312         understanding and remaining questions. *Cardiovascular Research* 2012; 96:234-243.

313     4. Koskinas KC, Sukhova GK, Baker AB, Papafaklis MI, Chatzizisis YS, Coskun AU, Quillard T, Jonas  
314         M, Maynard C, Antoniadis AP, Shi GP, Libby P, Edelman ER, Feldman CL, Stone PH. Thin-Capped  
315         Atheromata with Reduced Collagen Content in Pigs Develop in Coronary Arterial Regions  
316         Exposed to Persistently Low Endothelial Shear Stress. *Arterioscler Thromb Vasc Biol*  
317         2013;33(7):1494-1504.

318     5. Stone PH, Saito S, Takahashi S, Makita Y, Nakamura S, Kawasaki T, Takahashi A, Katsuki T,  
319         Nakamura S, Namiki A, Hirohata A, Matsumura T, Yamazaki S, Yokoi H, Tanaka S, Otsuji S,  
320         Yoshimachi F, Honye J, Harwood D, Reitman M, Coskun AU, Papafaklis MI, Feldman CL,  
321         PREDICTION Investigators. Prediction of Progression of Coronary Artery Disease and Clinical  
322         Outcomes Using Vascular Profiling of Endothelial Shear Stress and Arterial Plaque  
323         Characteristics. The PREDICTION Study. *Circulation* 2012;126:172-181.

324     6. Morbiducci U, Ponzini R, Rizzo G, Cadioli M, Esposito A, Montevecchi FM, Redaelli A.  
325         Mechanistic insight into the physiological relevance of helical blood flow in the human aorta.  
326         An in vivo study. *Biomech Model Mechanobiol* 2011;10:339-355.

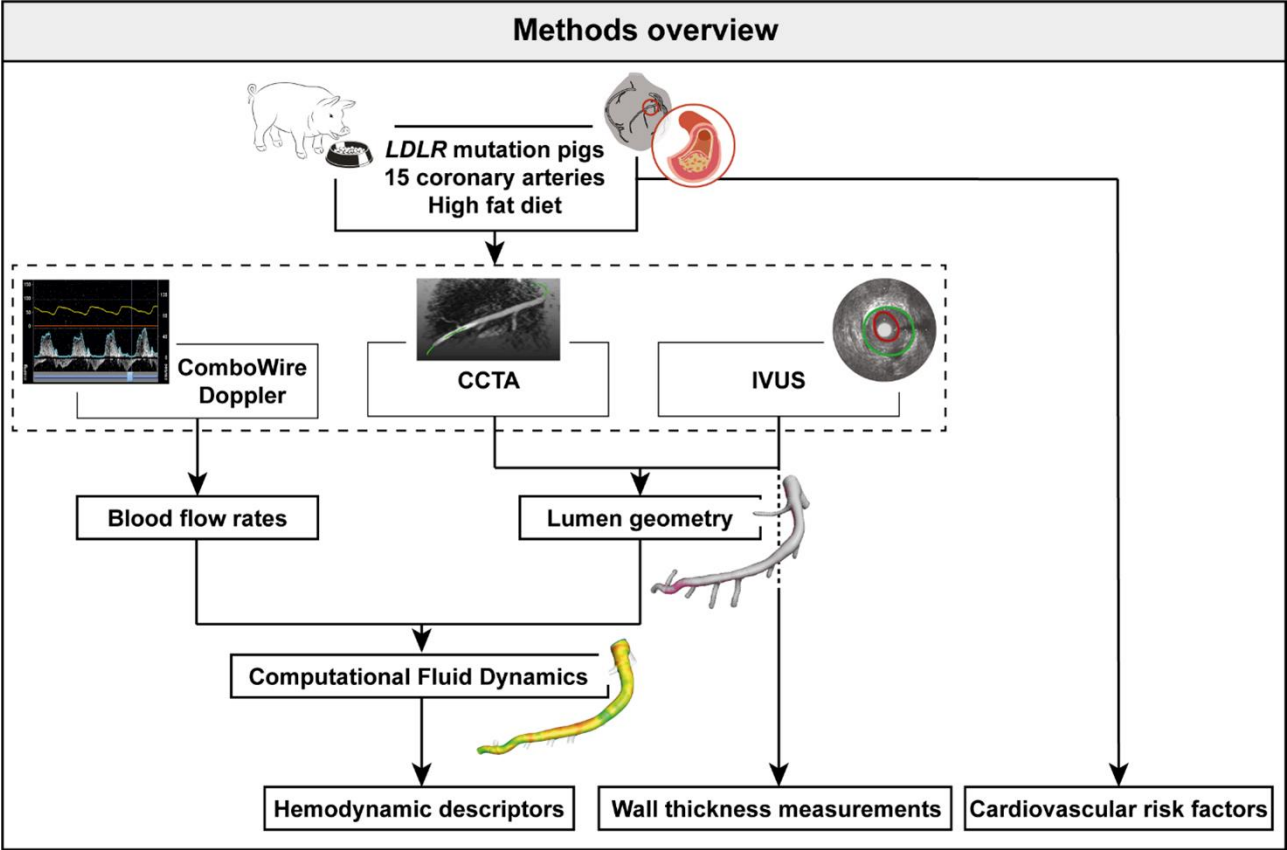
327     7. Liu X, Sun A, Fan Y, Deng X. Physiological significance of helical flow in the arterial system and  
328         its potential clinical applications. *Ann Biomed Eng* 2015;43(1):3-15.

- 329 8. Stonebridge PA, Hoskins PR, Allan PL, Belch JF. Spiral laminar flow in vivo. Clin Sci  
330 1996;91(1):17-21.
- 331 9. Stonebridge PA, Suttie SA, Ross R, Dick J. Spiral Laminar Flow: a Survey of a Three-Dimensional  
332 Arterial Flow Pattern in a Group of Volunteers. Eur J Vasc Endovasc Surg 2016;52(5):674-680.
- 333 10. Liu X, Pu F, Fan Y, Deng X, Li D, Li S. A numerical study on the flow of blood and the transport of  
334 LDL in the human aorta: the physiological significance of the helical flow in the aortic arch. Am J  
335 Physiol Heart Circ Physiol 2009;297:H163-H170.
- 336 11. Morbiducci U, Ponzini R, Rizzo G, Cadioli M, Esposito A, De Cobelli F, Del Maschio A,  
337 Montevecchi FM, Redaelli A. In vivo quantification of helical blood flow in human aorta by time-  
338 resolved three-dimensional cine phase contrast MRI. Ann Biomed Eng 2009;37:516-531.
- 339 12. Morbiducci U, Ponzini R, Gallo D, Bignardi C, Rizzo G. Inflow boundary conditions for image-  
340 based computational hemodynamics: impact of idealized versus measured velocity profiles in  
341 the human aorta. J Biomech 2013;46:102-109.
- 342 13. Gallo D, Steinman DA, Bijari PB, Morbiducci U. Helical flow in carotid bifurcation as surrogate  
343 marker of exposure to disturbed shear. J Biomech 2012;45:2398-2404.
- 344 14. Gallo D, Steinman DA, Morbiducci U. An Insight into the Mechanistic Role of the Common  
345 Carotid Artery on the Hemodynamics at the Carotid Bifurcation. Ann Biomed Eng 2015;43:68.
- 346 15. Gallo D, Bijari PB, Morbiducci U, Qiao Y, Xie Y, Etesami M, Haabets D, Lakatta EG, Wasserman  
347 BA, Steinman DA. Segment-specific associations between local haemodynamic and imaging  
348 markers of early atherosclerosis at the carotid artery: an in vivo human study. J R Soc Interface  
349 2018;15:20180352.
- 350 16. De Nisco G, Kok AM, Chiastra C, Gallo D, Hoogendoorn A, Migliavacca F, Wentzel JJ, Morbiducci  
351 U. The Atheroprotective Nature of Helical Flow in Coronary Arteries. Ann Biomed Eng  
352 2019;47(2):425-438.
- 353 17. Markl M, Schnell S, Wu C, Bollache E, Jarvis K, Barker AJ, Robinson JD, Rigsby CK. Advanced flow  
354 MRI: emerging techniques and applications. Clin Radiol 2016;71(8):779-95.

- 355 18. Hoogendoorn A, Kok AM, Hartman EMJ, De Nisco G, Casadonte L, Chiastra C, Coenen A,  
356 Korteland SA, Van der Heiden K, Gijzen FJH, Duncker DJ, van der Steen AFW, Wentzel JJ,  
357 Multidirectional wall shear stress promotes advanced coronary plaque development –  
358 comparing five shear stress metrics. *Cardiovasc Res* 2019;cvz212  
359 <https://doi.org/10.1093/cvr/cvz212>.
- 360 19. National Research Council (US). Committee for the Update of the Guide for Care and Use of  
361 Laboratory Animals, Guide for the Care and Use of Laboratory Animals (8<sup>th</sup> ed.). Washington,  
362 DC: National Academies Press (US), 2011.
- 363 20. Huo Y, Kassab GS. Intraspecific scaling laws of vascular trees. *J R Soc Interface* 2012;9(66):190-  
364 200.
- 365 21. Morbiducci U, Ponzini R, Grigioni M, Redaelli A. Helical flow as fluid dynamic signature for  
366 atherogenesis in aortocoronary bypass. A numeric study. *J Biomech* 2007;40:519-534.
- 367 22. Morbiducci U, Gallo D, Cristofanelli S, Ponzini R, Deriu MA, Rizzo G, Steinman DA. A rational  
368 approach to defining principal axes of multidirectional wall shear stress in realistic vascular  
369 geometries, with application to the study of the influence of helical flow on wall shear stress  
370 directionality in aorta. *J Biomech* 2015;48(6):899-906.
- 371 23. Malek AM, Alper SL, Izumo I. Hemodynamic shear stress and its role in atherosclerosis. *JAMA*.  
372 1999;282:2035-2042.
- 373 24. Chatzizisis YS, Coskun AU, Jonas M, Edelman ER, Feldman CL, Stone PH. Role of Endothelial  
374 Shear Stress in the Natural History of Coronary Atherosclerosis and Vascular Remodeling. *J Am*  
375 *Coll Cardiol* 2007;49:2379-93.
- 376 25. Fox B, James K, Morgan B, Seed WA. Distribution of fatty and fibrous plaques in young human  
377 coronary arteries. *Atherosclerosis*. 1982;41:337-347.
- 378 26. Nakashima T, Iwanaga Y, Nakaura Y. Pathologic study of hypertensive heart. *Acta Pathologica*  
379 *Japonica*. 1964;14(1):129-141.
- 380 27. Nakashima T, Tashiro T. Early morphologic stage of human coronary atherosclerosis. *Kurume*  
381 *Med J*. 1968;15(4):235-42.

- 382 28. Sabbah HN, Walburn FJ, Stein PD. Patterns of flow in the left coronary artery. J Biomech Eng.  
383 1984;106(3):272-9.
- 384 29. Torii R, Keegan J, Wood NB, Dowsey AW, Hughes AD, Yang GZ, Firmin DN, Thom SA, Xu XY. MR  
385 image-based geometric and hemodynamic investigation of the right coronary artery with  
386 dynamic vessel motion. Ann Biomed Eng 2010;38:2606-2620.
- 387 30. Winkel LC, Hoogendoorn A, Xing R, Wentzel JJ, Van der Heiden K. Animal models of surgically  
388 manipulated flow velocities to study shear stress-induced atherosclerosis. Atherosclerosis.  
389 2015;241:100-110.
- 390 31. Frydrychowicz A., Berger A, Munoz Del Rio A, Russe MF, Bock J, Harloff A, Markl M.  
391 Interdependencies of aortic arch secondary flow patterns, geometry, and age analysed by 4-  
392 dimensional phase contrast magnetic resonance imaging at 3 Tesla. Eur. Radiol.  
393 2012;22(5):1122-30.
- 394 32. Harloff A, Albrecht F, Spreer J, Stalder AF, Bock J, Frydrychowicz A, Schöllhorn J, Hetzel A,  
395 Schumacher M, Hennig J, Markl M. 3D blood flow characteristics in the carotid artery  
396 bifurcation assessed by flow-sensitive 4D MRI at 3T. Magn Reson Med 2009;61(1):65-74.
- 397 33. Schäfer M, Barker AJ, Kheyfets V, Stenmark KR, Crapo J, Yeager ME, Truong U, Buckner JK,  
398 Fenster BE, Hunter KS. Helicity and Vorticity of Pulmonary Arterial Flow in Patients With  
399 Pulmonary Hypertension: Quantitative Analysis of Flow Formations. J Am Heart Assoc.  
400 2017;6(12):e007010.
- 401 34. Oechtering TH, Sieren MM, Hunold P, Hennemuth A, Huellebrand M, Scharfschwerdt M,  
402 Richardt D, Sievers HH, Barkhausen J, Frydrychowicz A. Time-resolved 3-dimensional magnetic  
403 resonance phase contrast imaging (4D Flow MRI) reveals altered blood flow patterns in the  
404 ascending aorta of patients with valve-sparing aortic root replacement. J Thorac Cardiovasc  
405 Surg. 2019;S0022-5223(19)30773-1.
- 406 35. Brandts A, Roes SD, Doornbos J, Weiss RG, de Roos A, Stuber M, Westenberg JJ. Right coronary  
407 artery flow velocity and volume assessment with spiral k-space sampled breathhold velocity-  
408 encoded MRI at 3 tesla: accuracy and reproducibility. J Magn Reson Imaging. 2010;31(5):1215-  
409 1223.

- 410 36. Keegan J, Gatehouse PD, Mohiaddin RH, Yang GZ, Firmin DN. Comparison of spiral and FLASH  
411 phase velocity mapping, with and without breath-holding, for the assessment of left and right  
412 coronary artery blood flow velocity. *J Magn Reson Imaging*. 2004;19(1):40-49.
- 413 37. Johnson K, Sharma P, Oshinski J. Coronary artery flow measurement using navigator echo gated  
414 phase contrast magnetic resonance velocity mapping at 3.0 T. *J Biomech*. 2008;41(3):595-602.
- 415 38. Jahnke C, Manka R, Kozerke S, Kozerke S, Schnackenburg B, Gebker R, Marx N, Paetsch I.  
416 Cardiovascular magnetic resonance profiling of coronary atherosclerosis: vessel wall  
417 remodelling and related myocardial blood flow alterations. *Eur Heart J Cardiovasc Imaging*.  
418 2014;15(12):1400-1410.
- 419 39. Nagel E, Thouet T, Klein C, Schalla S, Bornstedt A, Schnackenburg B, Hug J, Wellnhofer E, Fleck  
420 E. Noninvasive determination of coronary blood flow velocity with cardiovascular magnetic  
421 resonance in patients after stent deployment. *Circulation*. 2003;107(13):1738-1743.



424  
425 **Figure 1. Schematic diagram of the study design, showing how imaging data contribute to define**  
426 **vessel geometry and hemodynamic variables.** *LDRL*: low-density lipoprotein receptor; *CCTA*:  
427 *coronary computed tomography angiography*; *IVUS*: *intravascular ultrasound*.

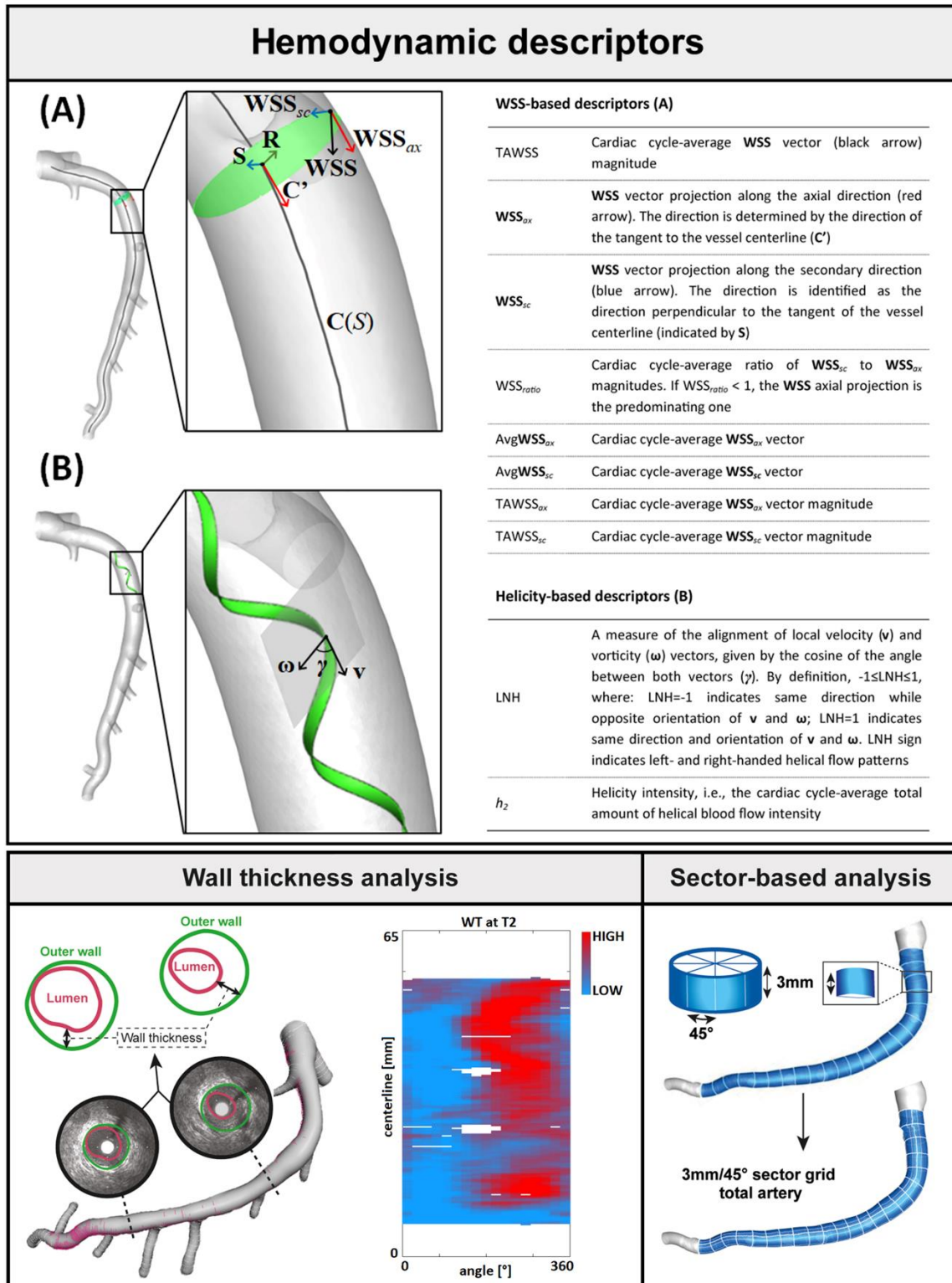


**Figure 2. Methodology of hemodynamic descriptors and wall thickness (WT) assessment and analysis. Hemodynamic descriptors panel** - Figure (A): example of **WSS** vector acting in a generic point at the luminal surface. Its axial (**WSS<sub>ax</sub>**) and secondary (**WSS<sub>sc</sub>**) components are also displayed. **C(S)**: vessel centerline; **C'**: vector tangent to the centerline; **R**: vector perpendicular to **C'** directed from the centerline to the generic point at the arterial surface; **S**: vector orthogonal to vectors **R** and **C'**. Table (A): WSS-based descriptors involved in the analysis. A short caption for each descriptor is provided. Figure (B): example of the helical-shaped trajectory described by an element of blood moving within the coronary artery.  $\gamma$  is the angle between local velocity (**v**) and vorticity (**ω**) vectors ( $\text{LNH} = \cos(\gamma)$ ). Table (B): helicity-based descriptors involved in the analysis. A short caption for each descriptor is provided. **Wall thickness analysis panel** - Example of lumen (pink contour) and vessel outer wall (green contour) segmentation on two IVUS frames of an explanatory case. The obtained 2D distribution of WT at T2 is also shown. The angle indicates the circumferential direction around the arterial lumen. The top of the graph is the proximal region and the bottom of the graph the distal region of the artery. **Sector-based analysis panel** - Example of IVUS-imaged segment (blue colored) region in 3mm/45 degrees luminal sectors for an explanatory case.



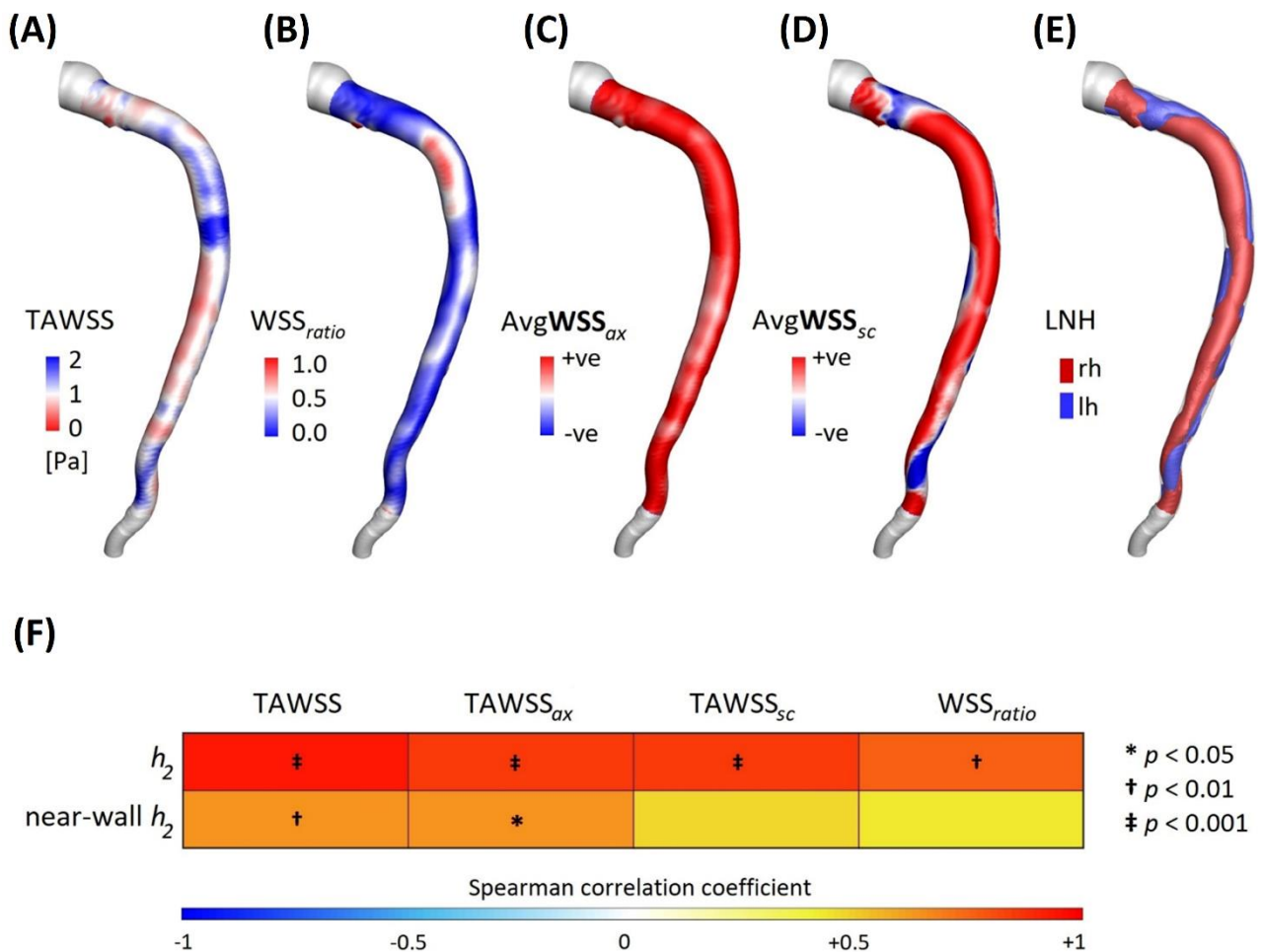


**Figure 3. Coronary hemodynamics: general observations and link between hemodynamic variables.** (A)-(D) WSS-based descriptors distribution at the luminal surface of a representative LAD coronary artery (a) (see Figure S1 of the Supplementary Materials). For the same explanatory case, visualization of LNH cycle-average isosurfaces is also provided in panel (E). For TAWSS ( $WSS_{ratio}$ ), the low (red) and high (blue) values are indicated. For cycle-average axial ( $AvgWSS_{ax}$ ) WSS vector projections, colors identify the forward (red) and backward (blue) flow direction, respectively. As for LNH, also for the cycle-average secondary ( $AvgWSS_{sc}$ ) WSS vector projections blue and red colors identify the left and right-handed direction, respectively. +ve: positive; -ve: negative; rh: right-handed; lh: left-handed. (F) Spearman correlation coefficients between WSS-based and helicity-based descriptors. The average value of the hemodynamic descriptors for each individual case was considered. For statistically significant relations,  $p$  values are also reported.

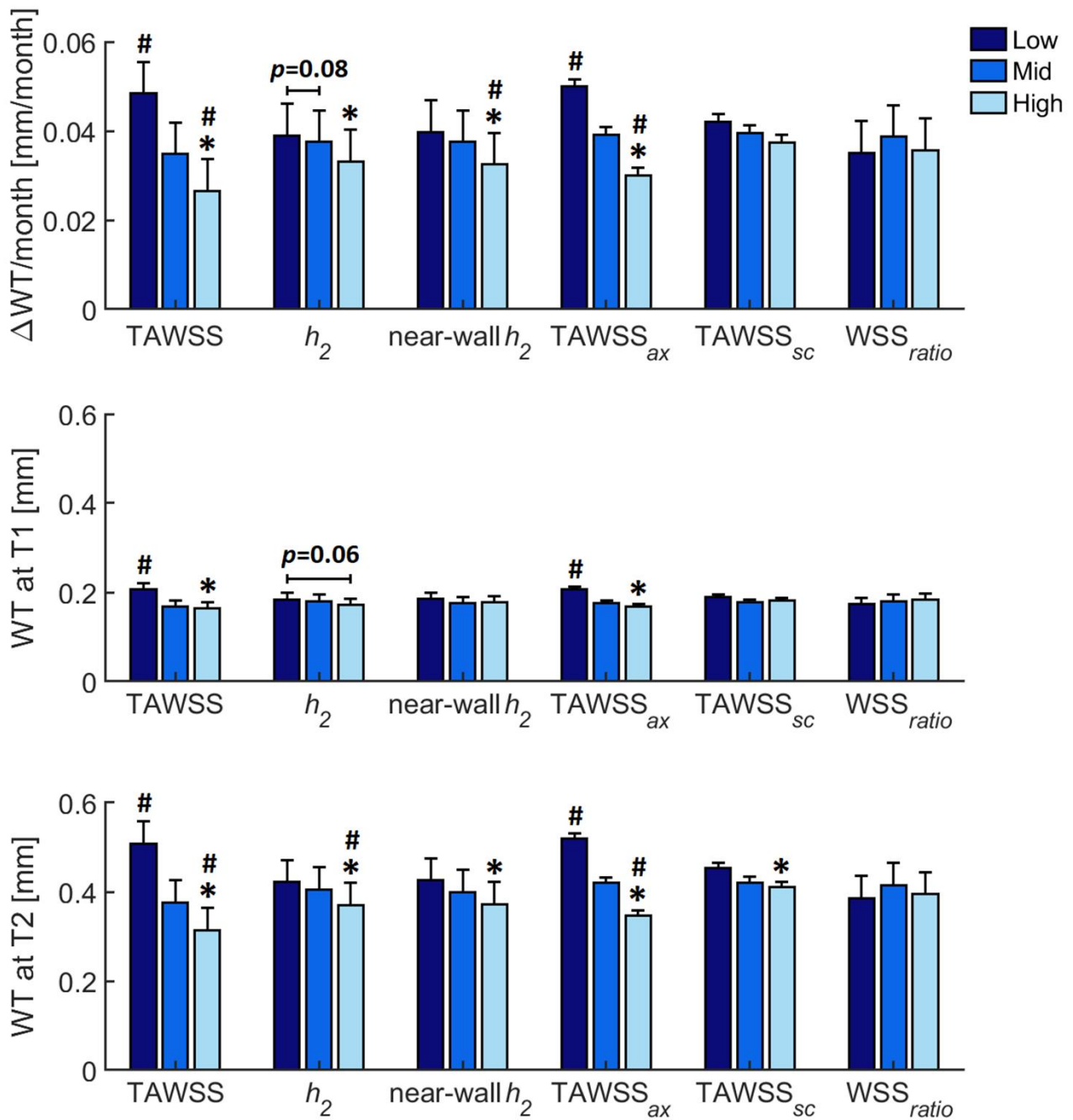


**Figure 4. Link between hemodynamic variables and increase in wall thickness.** Relationship between baseline (T1) hemodynamic descriptor levels and 1) estimated plaque growth per month (top panel), 2) WT at T1 (middle panel), and 3) WT at T2 (bottom panel). Estimated mean and standard error of the mean (SEM) values are reported. The hemodynamic descriptors were divided in low (dark blue bars), mid (blue bars) and high (light blue bars) tertiles per artery. The average value of the hemodynamic descriptors and WT measurements in the 3mm/45 degrees sectors was considered. \* $p < 0.05$  compared to low tertile, # $p < 0.05$  compared to the mid tertile of all parameters.

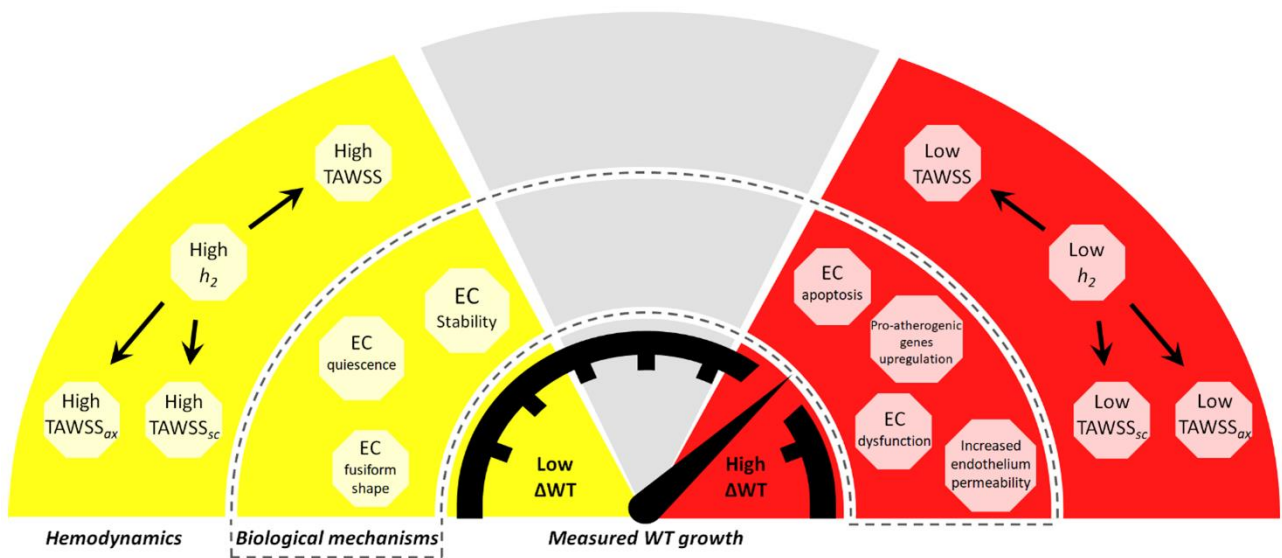


**Figure 5. Schematic of the main findings of the study and the relationship with biological mechanisms related to atherosclerosis**